The core domain as the force sensor of the yeast mechanosensitive TRP channel

Zhenwei Su,[1] Andriy Anishkin,[3] Ching Kung,[1,2] and Yoshiro Saimi[1]

[1]Laboratory of Molecular Biology and [2]Department of Genetics, University of Wisconsin-Madison, Madison, WI 53706
[3]Department of Biology, University of Maryland, College Park, MD 20742

Stretch-activated conductances are commonly encountered in careful electric recordings. Those of known proteins (TRP, MscL, MscS, K_{2p}, Kv, etc.) all share a core, which houses the ion pathway and the gate, but no recognizable force-sensing domain. Like animal TRPs, the yeast TRPY1 is polymodal, activated by stretch force, Ca^{2+}, etc. To test whether its S5–S6 core senses the stretch force, we tried to uncouple it from the peripheral domains by strategic peptide insertions to block the covalent core–periphery interactions. Insertion of long unstructured peptides should distort, if not disrupt, protein structures that transmit force. Such insertions between S6 and the C-terminal tail largely removed Ca^{2+} activation, showing their effectiveness. However, such insertions as well as those between S5 and the N-terminal region, which includes S1–S4, did not significantly alter mechanosensitivity. Even insertions at both locations flanking the S5–S6 core did not much alter mechanosensitivity. Tryptophan scanning mutations in S5 were also constructed to perturb possible noncovalent core–periphery contacts. The testable tryptophan mutations also have little or no effects on mechanosensitivity. Boltzmann fits of the wild-type force–response curves agree with a structural homology model for a stretch-induced core expansion of ~2 nm^2 upon opening. We hypothesize that membrane tension pulls on S5–S6, expanding the core and opening the TRPY1 gate. The core being the major force sensor offers the simplest, though not the only, explanation of why so many channels of disparate designs are mechanically sensitive. Compared with the bacterial MscL, TRPY1 is much less sensitive to force, befitting a polymodal channel that relies on multiple stimuli.

The Journal of General Physiology

INTRODUCTION

Mechanosensitive (MS) ion channels are major first-line force sensors in a variety of force-related physiological processes from osmotic regulation to hearing and touch sensations. Force-activated conductances have been observed in various preparations since its first demonstration in cultured muscle cells (Guharay and Sachs, 1984). MS channels of known sequences are widespread among diverse channel families, including the prokaryotic MscL and MscS (Sukharev et al., 1997; Booth et al., 2007; Kung et al., 2010) and the eukaryotic ENaC (Chalfie, 2009), K_{2P} (Honoré, 2007), and TRP channels (Christensen and Corey, 2007). Several eukaryotic channels that are better known for sensing other stimuli are also found to be mechanosensitive under patch clamp, such as Kv (Gu et al., 2001; Schmidt and MacKinnon, 2008), Nav (Shcherbatko et al., 1999; Morris and Juranka, 2007; Beyder et al., 2010), Cav (Calabrese et al., 2002), HCN2 (Lin et al., 2007), BK (Zhao et al., 2010), NMDA receptor (Kloda et al., 2007), and even CFTR (Zhang et al., 2010). These disparate MS channels share no recognizable force-sensing motifs with conserved protein sequences comparable to the well-recognized voltage-sensing domain or various ligand-binding pockets.

How force activates MS channels is a crucial question in this field of study (Kung, 2005; Arnadóttir and Chalfie, 2010). Clearer molecular insights come from the study of prokaryotic MscL and MscS. They receive force through the membrane tension (Sukharev et al., 1997; Kung, 2005). They are homomultimers of subunits with two or three transmembrane helices forming the core domain that harbors the ion conduction pathway and the channel gate. Membrane tension pulls these transmembrane helices, triggering the core expansion and subsequent gate opening of MscL and MscS. There are no separate force-sensing domains besides the core.

On the other hand, it remains unclear how force activates eukaryotic MS channels in molecular terms (Arnadóttir and Chalfie, 2010). In principle, the source of force can either come from membrane bilayer, like MscL and MscS (Sukharev et al., 1997; Kung, 2005), or from extracellular matrix/cytoskeleton (Christensen and Corey, 2007; Arnadóttir and Chalfie, 2010), or can be indirectly conveyed by diffusible elements (Vriens et al., 2004). Cytoskeletons can negatively regulate the mechanosensitivity of MS channels by relaxing the local membrane tension surrounding MS channels (Sharif-Naeini et al., 2009; Sachs, 2010). There are reports of eukaryotic MS channels being reconstituted into pure lipids

Correspondence to Yoshiro Saimi: ysaimi@wisc.edu

The Rockefeller University Press $30.00
J. Gen. Physiol. Vol. 138 No. 6 627–640
www.jgp.org/cgi/doi/10.1085/jgp.201110693

and still retaining mechanosensitivity, such as NMDA receptor (Kloda et al., 2007). Others, such as TRPY1 (Zhou et al., 2003), TRPV4 (Loukin et al., 2010) of the TRP channel family, TREK1 (Honoré, 2007) of the K_{2P} family, and CFTR (Zhang et al., 2010), have been shown to be mechanosensitive in excised patches in simple salt solutions and thus are most likely to receive force also from membrane lipids. This principle is also made clear with the gramicidin A model (Lundbæk et al., 2004, 2010). Common to all channels is the presence of the core domain that harbors the selectivity filter, ion pathway, and the gate. In want of a common force-sensing structure, the core domain of these eukaryotic channels may also serve as the membrane force sensor.

To explore this possibility, here we use the yeast MS TRP channel (Fig. S1), TRPY1, and quantitatively studied the molecular mechanism of its force activation. TRPY1 responds to hyperosmotic shocks in vivo (Denis and Cyert, 2002) and presents a 320-pS unitary conductance upon stretching of excised patches bathed in symmetrical 180-mM KCl (Zhou et al., 2003). Much like Kv, each TRP channel is likely a tetramer of subunits, each comprising six transmembrane helices (S1–S6), although crystal structures are not yet available. The four S5–S6s are presumed to converge to form the core domain, whereas S1–S4s likely form peripheral modules attached to the core. By analogy to the crystal structure of Kv in membrane (Long et al., 2007), the core domain and S1–S4 both have extensive access to membrane lipids and therefore can sense membrane tension. We wish to test whether the membrane force is sensed by S1–S4, by the core domain, or both. S1–S4 deletions or chimeras with S5–S6 flanked by foreign S1–S4 could provide a clear indication. However, several such constructs yielded no functional channels (unpublished data). We therefore attempted to uncouple the core domain by disrupting the covalent couplings from the peripheral domains to the core with strategically inserted peptides. Tryptophan scanning mutants in S5 were also constructed to perturb possible noncovalent core–periphery contacts.

MATERIALS AND METHODS

Yeast strains and cultures

The wild-type parental strains were BY4742 (*MATα his3Δ leu2Δ lys2Δ ura3Δ*) and *trpy1*Δ mutant (chromosomal knockout strain YOR088W; *trpy1::km*). For electrophysiology, standard yeast media with yeast extract, peptone, and dextrose was used (Zhou et al., 2003; Su et al., 2009).

Mutagenesis

All site-directed mutagenesis were performed using the standard overlap extension PCR method (Ho et al., 1989). Different PCR fragments carrying the corresponding mutations were cloned into HindIII–XhoI sites of *TRPY1* in a prYVC plasmid carrying a strong constitutively active promoter, the glyceraldehyde-3-phosphate dehydrogenase promoter, and a *URA3* marker. All mutations were verified by sequencing. Sequenced plasmids were linearized by EagI–MluI before transforming into *trpy1Δ* for gene integration into the chromosome. Transformed yeast mutant strains with correct markers were sequenced again from the genome to verify the *trpy1* mutant integrants. All experiments were performed on these integrants. Wild-type control for ensemble current analysis was constructed the same way as the mutants. For wild-type single-channel analysis, a weak native promoter was used to replace the glyceraldehyde-3-phosphate dehydrogenase promoter to achieve low expression.

Solutions

For patch-clamp recordings, the pipette solution contained 150 mM KCl, 5 mM $MgCl_2$, 300 mM sorbitol, and 10 mM HEPES-KOH, pH 7.2. The bath solution contained 150 mM KCl, 5 mM $MgCl_2$, 300 mM sorbitol, 10 mM HEPES-KOH, pH 7.2, and different Ca^{2+} concentrations adjusted with $CaCl_2$ and EGTA. For $[Ca^{2+}]$ above 10^{-5} M, $CaCl_2$ was directly added to EGTA-free bath solution. For $[Ca^{2+}]$ below 10^{-5} M, appropriate amounts of $CaCl_2$ recommended by Maxchelator software were added to the bath solution containing 1–2 mM EGTA. For the 0 Ca^{2+} solution, 10 mM EGTA was added to the solution without additional Ca^{2+}.

Electrophysiology

Yeast vacuoles were generated as previously described (Su et al., 2007; Zhou et al., 2007). All patch-clamp recordings were performed with Clampex 10.0 (Axon Instruments). Data were sampled at 5 kHz and filtered at 1–5 kHz. The data were further filtered at 1 kHz before analysis using a digital filter (Clampfit; Axon Instruments) as necessary. 100-µl glass pipettes (Drummond Scientific Company) were pulled with a micropipette puller (P-97; Sutter Instrument) to so-called bubble numbers strictly measured to be between 4.5 and 5.1 in ethanol (Sakmann and Neher, 1983). With negative pressure in the pipette, 2–3-GΩ seals were formed before being broken by transient voltage pulses to reach the whole-vacuole mode. Whole-vacuole mode patches were subsequently excised into the cytoplasmic-side-out mode. Data were acquired at −50 mV, with the cytoplasmic side being negative. Bath perfusion was used to change $[Ca^{2+}]$. Mechanical stimulation was applied as pressure exerted with a 60-ml syringe, and the pressure was monitored with a pressure sensor (PX140; Omega). Experiments were performed at room temperature (21–23°C). Data were analyzed using Clampfit 10.0 (Axon Instruments). Leak currents measured by applying pressure at 0 $[Ca^{2+}]$ were negligible. For ensemble current analyses, saturation levels were the current maxima with much reduced noise level at high $[Ca^{2+}]$ and high pressure. In mutants with frequent flickers, saturations were judged by the lack of high pressure–induced additional current at high $[Ca^{2+}]$, assuming that these two energies are synergistically summed. Open probability (P_o) was calculated as the percentage of the saturation. In single-channel patches, P_o was also calculated from the flat-top events.

Statistical analysis

Data are presented as means ± SD. Curves were fitted with SigmaPlot 10.0 (Systat Software). A one-tail unpaired Student's *t* test was performed with Excel (Microsoft) to examine statistical differences. $P < 0.05$ is considered significantly different.

Structural modeling

We used the ROSETTA software (Simons et al., 1997) to model the pore domain of TRPY1 (Zhou et al., 2007). The complete details on the modeling procedure, the features of the proposed models, and videos illustrating the suggested gating motion are presented in the web supplement to the original publication (Zhou et al., 2007). In brief, the models (see Fig. 8) were based on the remote homology to K^+ channels of the shaker family. The initial model was an open state with an architecture of the pore domain (S5–S6) closely following KvAP structure resolved in the open

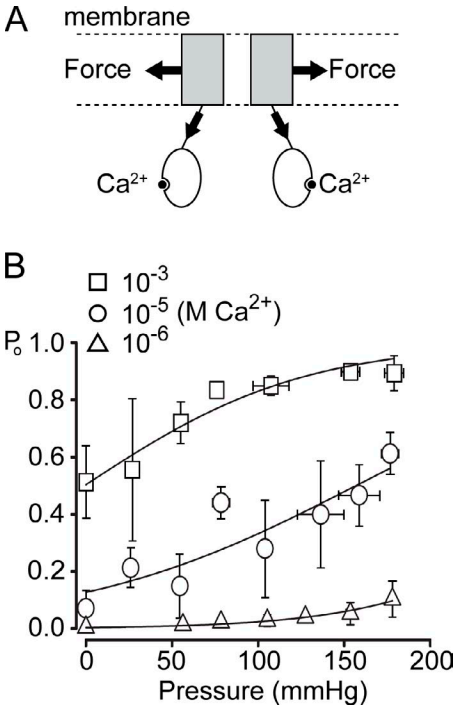

Figure 1. Bimodal activation of TRPY1. (A) A diagram showing that TRPY1 senses membrane stretch force through the membrane-embedded domains and Ca^{2+} through the cytoplasmic domains. Energetically, the open probability is governed by $\Delta G_0 - \Delta G_{force} - \Delta G_{Ca}{}^{2+}$, where ΔG_0 refers to the energy difference between the C and O state before the application of force or Ca^{2+}. ΔG_0 includes the energies from structures, temperature, protonation, etc. (B) The P_o versus pressure plots at different $[Ca^{2+}]$. For each of the three $[Ca^{2+}]$, P_o from TRPY1 ensemble currents is plotted against the applied pressure and fitted with the following Boltzmann equation: $P_o = 1/[1 + a \times \exp(-\Delta\alpha \times P)]$, which is transformed from $P_o = 1/[1 + \exp((\Delta E - \gamma \times \Delta A)/k_B \times T)]$, where a and $\Delta\alpha$ are fitting parameters in the P_o–pressure plot, with $\Delta\alpha$ (in millimeters of Hg^{-1}) being the slope parameter; P (in millimeters of Hg) is the applied pressure; ΔE is the free energy of the channel at given $[Ca^{2+}]$; γ (in Newtons per meter) is the membrane tension; ΔA (in square meters) is the expansion coefficient; k_B is the Boltzmann constant; and T is the absolute temperature. The transformation assumes that the radius of our patches, r (in meters), remains constant. We strictly controlled the sizes of our pipette tips in a narrow range with the bubble numbers 4.5–5.1 in ethanol(Sakmann and Neher, 1983) to approach the constancy of r. With this assumption, γ can be converted to P according to Laplace's law. The saturation levels of channel activities were determined by applying high pressure at high $[Ca^{2+}]$ (10^{-3} M). See Materials and methods for details. Although $[Ca^{2+}]$ laterally shifts P_o–pressure curves, all three fits have a similar $\Delta\alpha$ value (Table I), indicating that $\Delta\alpha$ defines the mechanosensitivity and is independent of $[Ca^{2+}]$. Means ± SD (not SEM; $n = 4$ for 10^{-3} M, $n = 6$ for 10^{-5} M, and $n = 4$ for 10^{-6} M Ca^{2+}).

state. To represent the closed state, the cytoplasmic part of the model (including the gate region and lipid interface–exposed aromatic residues) was modified to follow the closed KcsA structure. Note that explicit membrane tension was not included in building the models, and the difference in the expansion area between the closed and open state was essentially dictated by the two known distinct templates representing open and closed conformations of tetrameric potassium channels. The models were energy minimized, relaxed, and symmetry annealed in short molecular dynamics simulations.

TABLE I

Slope parameters ($\Delta\alpha$) extracted from ensemble current analyses

Constructs	$[Ca^{2+}]$	Slope parameter $\Delta\alpha$ (mean ± SD)	No. of patches
	M	*$mmHg^{-1}$*	
WT	10^{-3}	0.015 ± 0.0043	4
WT	10^{-5}	0.016 ± 0.0050	6
WT	10^{-6}	0.018 ± 0.0031	4
358–486-12GGS	10^{-5}	0.012 ± 0.0033	4

The ensemble current plots of P_o versus pressure from wild type at different $[Ca^{2+}]$ (10^{-6}, 10^{-5}, and 10^{-3} M) and 358–486-12GGS at intermediate $[Ca^{2+}]$ (10^{-5} M) were fitted with the Boltzmann equation: $P_o = 1/[1 + a \times \exp(-\Delta\alpha \times P)]$ (Fig. 1 B). The slope parameters, $\Delta\alpha$, of the wild type at different $[Ca^{2+}]$ are not significantly different (P = 0.38, 0.28, and 0.28 in a pairwise *t* test). $\Delta\alpha$ of 358–456-12GGS is also not significantly different from that of the wild type at 10^{-5} M Ca^{2+} (P = 0.07).

Online supplemental material

Fig. S1 shows a sequence comparison and a phylogenetic tree, which indicate the deep roots and loose connections among TRP channel subfamilies. Online supplemental material is available at http://www.jgp.org/cgi/content/full/jgp.201110693/DC1.

RESULTS

Synergistic activation of TRPY1 by stretch force and cytoplasmic $[Ca^{2+}]$

TRP channels are polymodal, responding to multiple stimuli (Voets et al., 2005). We have previously shown that TRPY1 is also synergistically activated by stretch through its transmembrane helices and by Ca^{2+} binding in the cytoplasmic domain with a DDDD motif (Fig. 1 A; Su et al., 2009). This is most likely a result of the allosteric effect of membrane force and Ca^{2+}, much like the allosteric activation of BK channels by both voltage and Ca^{2+} (Cui and Aldrich, 2000) and some of TRP channels by voltage, temperature, and chemicals (Latorre et al., 2007; Voets et al., 2007). Conceptually, TRPY1's P_o is determined by the energy intrinsic to the channel's structure at rest (ΔG_0) as well as gating energies from different modalities; the ones from force (ΔG_{force}) and Ca^{2+} (ΔG_{Ca}) are especially germane here. We directly measure TRPY1 activities in cytoplasmic-side-out patches excised from exposed vacuoles, clamped at −50 mV, and stretch the patch by measured pressures through the recording pipette. Without added pressure, the basal P_o is governed by $[Ca^{2+}]$. At extreme $[Ca^{2+}]$ (10^{-6} or 10^{-3} M) where the basal P_o is very low or very high, force activation by pipette pressure remains, although limited in magnitude (Fig. 1 B; and see Fig. 3 A), whereas a wide range of wild-type force activation is best displayed at an intermediate $[Ca^{2+}]$ of 10^{-5} M (Fig. 1 B; and see Fig. 3 A). $[Ca^{2+}]$ shifts the Boltzmann curve of P_o versus pressure laterally but does not significantly alter its slope ($\Delta\alpha = \sim 0.015$ $mmHg^{-1}$; Fig. 1 B and Table I). Thus, the mechanosensitivity of TRPY1 is

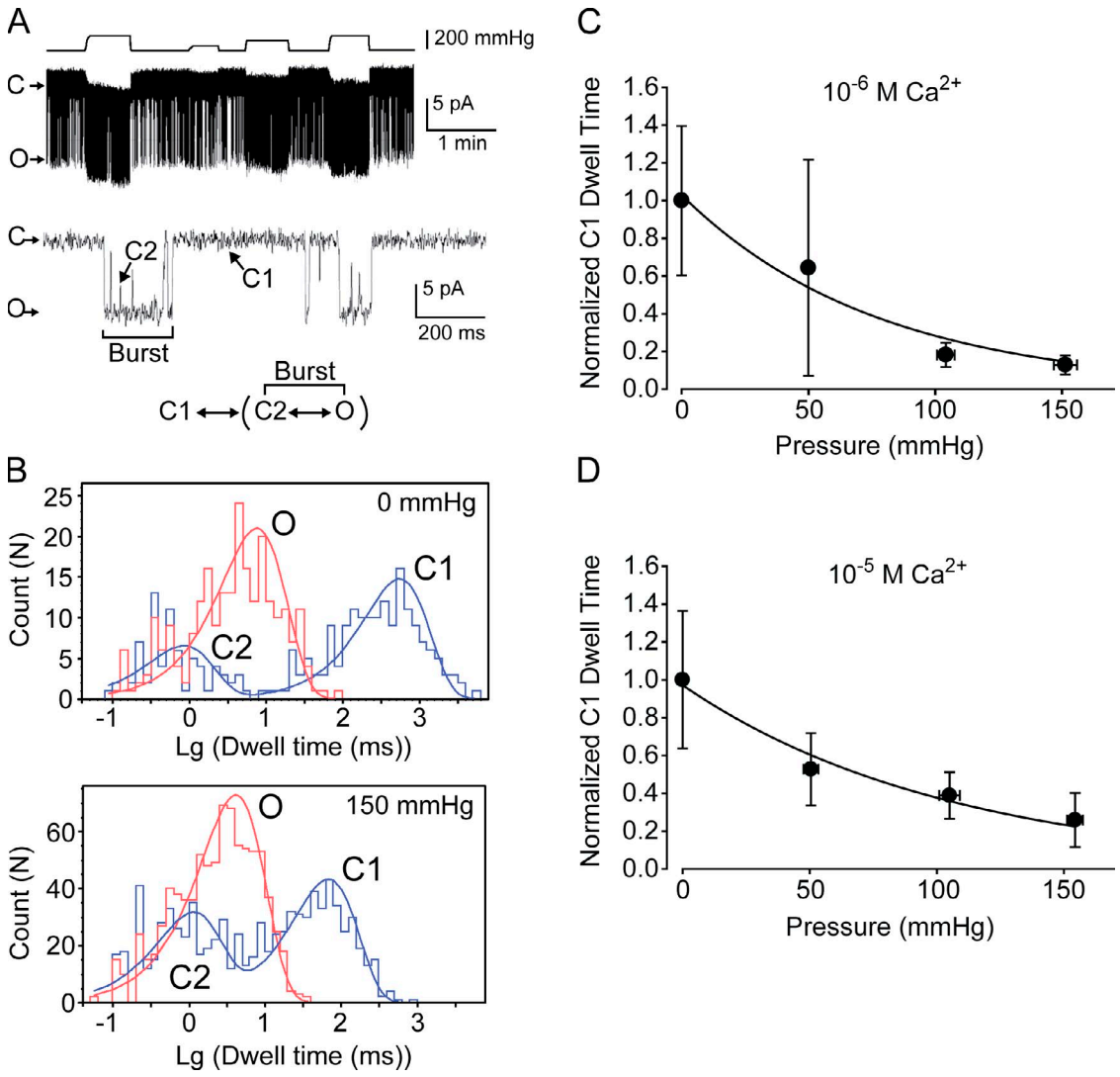

Figure 2. Single-channel analysis of the force activation indicating the C1 to burst transition step is mechanosensitive. (A, top) A single-channel recording at 10^{-6} M Ca^{2+} in response to different pressures over 5.5 min. (middle) An expanded view of a short portion in the top trace showing different states: an interburst closed state (C1), a burst state comprising an open state (O), and an intraburst closed state (C2). The recording presented here has higher basal P_o than average, which facilitated kinetics analysis. (bottom) A minimal kinetics model for TRPY1. (B) All-point histogram of A for dwell time analyses of different states without pressure (0 mmHg; top) and with 150 mmHg of pressure (bottom). The comparison shows that pressure mainly shortens C1 without much affecting O and C2. Also see Table II. (C) The normalized C1 dwell time to that of 0 mmHg of pressure is plotted against pressure at 10^{-6} M Ca^{2+} and fitted with an exponential equation: normalized C1 dwell time = $b \times \exp(-\Delta\alpha_k \times P)$, similar to that described in Fig. 1 B. The slope parameter $\Delta\alpha_k$ (Table III) here corresponds to the slope parameter $\Delta\alpha$ from the ensemble current analysis in Figs. 1 B and 3 F. (D) A plot similar to C at 10^{-5} M Ca^{2+}. Means ± SD (not SEM; $n = 5$ for 10^{-6} M and $n = 3$ for 10^{-5} M Ca^{2+}).

independent of $[Ca^{2+}]$. The mechanosensitivity of TRPY1, $\Delta\alpha$, should not be confused with the midpoint of the Boltzmann distribution or the threshold of channel activation, as these reflect the sum of ΔG_{Ca} and ΔG_0 for TRPY1.

Kinetics analyses of single TRPY1 activities

Single-channel analyses show that TRPY1 opens in bursts. Its kinetics can be summarized as C1↔[C2↔O], where the brackets delineate the burst state (Fig. 2 A). Within the burst, the order of O and C2 cannot be distinguished. Increasing pipette pressure mainly shortens the interburst closure, C1, with relatively small effects on the intraburst closure, C2, or the open dwell, O (Fig. 2 B and Table II). C1 shortens monotonously with pressure (Fig. 2, C and D). The plot of C1 dwell versus pressure yields a slope remarkably similar to the aforementioned $\Delta\alpha$ (Fig. 2, C and D; and Table III), indicating that the forward transition from C1 to the burst is the main mechanically sensitive step.

Insertions of long unstructured peptides after S6 effectively remove most of the Ca^{2+} activation

Although there is yet no reported crystallographic structure of the TRP channel, TRP is expected to have a domain arrangement similar to Kv (Long et al., 2005b,

TABLE II

Dwell time analysis of the wild-type single channel showing the effect of membrane stretch force on different states

$[Ca^{2+}]$	Normalized dwell times of different states under 150-mmHg pressure (mean ± SD)			No. of patches
	C1	C2	O	
M				
10^{-5}	0.21 ± 0.082	0.84 ± 0.24	1.3 ± 0.22	3
10^{-6}	0.13 ± 0.031	1.0 ± 0.59	1.9 ± 0.78	5

Dwell times in different states under 150-mmHg pressure at two different $[Ca^{2+}]$ normalized to those without pressure (Fig. 2 B, top). Unity would indicate no change. As shown clearly, C1 is significantly reduced by pressure, whereas C2 and O are mildly affected. Note that the missed short C2 likely caused an overestimation of O.

2007), in which S1–S4 forms a peripheral transmembrane domain connecting to the gate in the S5–S6 core through a short S4–S5 linker peptide. Also, the C-terminal cytoplasmic domain of TRPY1 harbors the Ca^{2+}-binding domain (Su et al., 2009). To test whether any of these peripheral domains senses the membrane stretch before transmitting the force to the gate, we engineered strategic insertions or substitutions in an attempt to uncouple the S5–S6 core from the neighboring domains. Such mutations are near or in the predicted gating structure of the core and are therefore expected to result in channels that have abnormally high (gain of function) or low (loss of function) basal activities. Although mechanosensitivity remains in these mutants, the range can become limited at the intermediate $[Ca^{2+}]$ of 10^{-5} M, the most suitable concentration in which to examine the wild-type channel. We therefore often adjusted the $[Ca^{2+}]$ for most mutants so as to display the mechanosensitivity of the mutants in near full range.

A 12-residue peptide, GGSGGSGGSGGS (henceforth called 12GGS), should produce an unstructured loop without a rigid or well-defined conformation. It is expected to greatly distort, if not completely disrupt, any regular covalent structures in a protein. The potency of such insertions is evident when placed in several positions between S6 and the C-terminal tails. Such insertions remove nearly all the TRPY1's sensitivity to Ca^{2+} (Su et al., 2009).

TABLE III

The slope parameters from the analysis of wild-type C1 dwell time

$[Ca^{2+}]$	Slope parameter $\Delta\alpha_k$ (mean ± SD)	No. of patches
M	$mmHg^{-1}$	
10^{-5}	0.011 ± 0.0038	3
10^{-6}	0.017 ± 0.0086	5

The single-channel plots of normalized C1 dwell time versus pressure from the wild type at different $[Ca^{2+}]$ (10^{-6} and 10^{-5} M) were fitted with an exponential equation: normalized C1 dwell time = $b \times \exp(-\Delta\alpha_k \times P)$ (Fig. 2). The slope parameter $\Delta\alpha_k$ here is remarkably similar to the slope parameter $\Delta\alpha$ from the ensemble current analysis in Table I, indicating that the transition from C1 to B is the major MS step.

For example, inserting this peptide at position 486 (called 486-12GGS) shortly after S6 (Fig. 3 B) yielded a mutant channel that is almost completely insensitive to Ca^{2+}, with an extremely low P_o (~2% in an overestimation) even at high $[Ca^{2+}]$ (10^{-3} M; Fig. 3 E, diamonds), in stark contrast to the ~65% P_o of wild type at 10^{-3} M Ca^{2+} (Fig. 3, A and E, circles). In contrast, when the force activation was examined at high $[Ca^{2+}]$ (10^{-3} M), 486-12GGS displayed a full range of mechanosensitivity like the wild type (Fig. 3 B).

Peptide insertions between S1–S4 and S5–S6

Given the dramatic effect of the 12GGS insertion at the C terminus of the S5–S6 core, we tested the effect of the same insertion at the N terminus of this core. In Kv, S1–S4 forms a peripheral domain connecting to the gate in the S5–S6 core through a short S4–S5 linker peptide. S1–S4 houses the voltage sensor, the movement of which is mechanically coupled to the gate (Long et al., 2005b). Sequence analyses suggest that Q359–K374 of TRPY1 forms an amphipathic helix that links S4 to S5, as in Kv (Long et al., 2005b, 2007). To test whether the S1–S4 peripheral domains likewise sense the membrane force before transmitting it to the gate through the linker, we inserted 12GGS at position 358 (358-12GGS) at the N terminus of the S4–S5 linker (Fig. 3 C). This insertion created a gain-of-function mutant, with a greatly increased basal P_o. At intermediate $[Ca^{2+}]$ (10^{-5} M), its basal P_o is already ~40% (Fig. 3 E, squares), compared with 3% from wild type. At high $[Ca^{2+}]$ (10^{-3} M), 358-12GGS opens to near saturation, obscuring force activation (Fig. 3 C, right). Adjusting $[Ca^{2+}]$ to lower levels revealed that 358-12GGS clearly remains sensitive to force (Fig. 3 C, left and middle traces).

To better uncouple the core domain, we inserted the aforementioned peptide at both sites flanking the core in an attempt to greatly distort or disrupt all covalent couplings between the core and the periphery. Like the 486-12GGS single insertant, this double-insertion mutant (358–486-12GGS) is almost insensitive to Ca^{2+} (Fig. 3 E, triangles). However, its basal activity is higher than that of wild type at lower $[Ca^{2+}]$ (10^{-6} or 10^{-5} M), much like the 358-12GGS single insertant. Thus, the double-insertion mutant appears to show a compensatory effect from the two single insertions. Importantly, at intermediate $[Ca^{2+}]$ (10^{-5} M), the 358–486-12GGS channel displays the full range of activation by force to near saturation (Fig. 3 D). The force activation of this double-insertion mutant was taken as a representative and analyzed in detail. Its P_o relationship to applied pressure was indistinguishable from that of the wild type (Fig. 3 F). The Boltzmann fits yielded values of $\Delta\alpha$ for the wild type and 358–486-12GGS with no significant difference (Table I).

The aforementioned results are not dependent on the specific nature of the GGSGGSGGSGGS peptide or the insertion site. We have tested 16 insertions of different

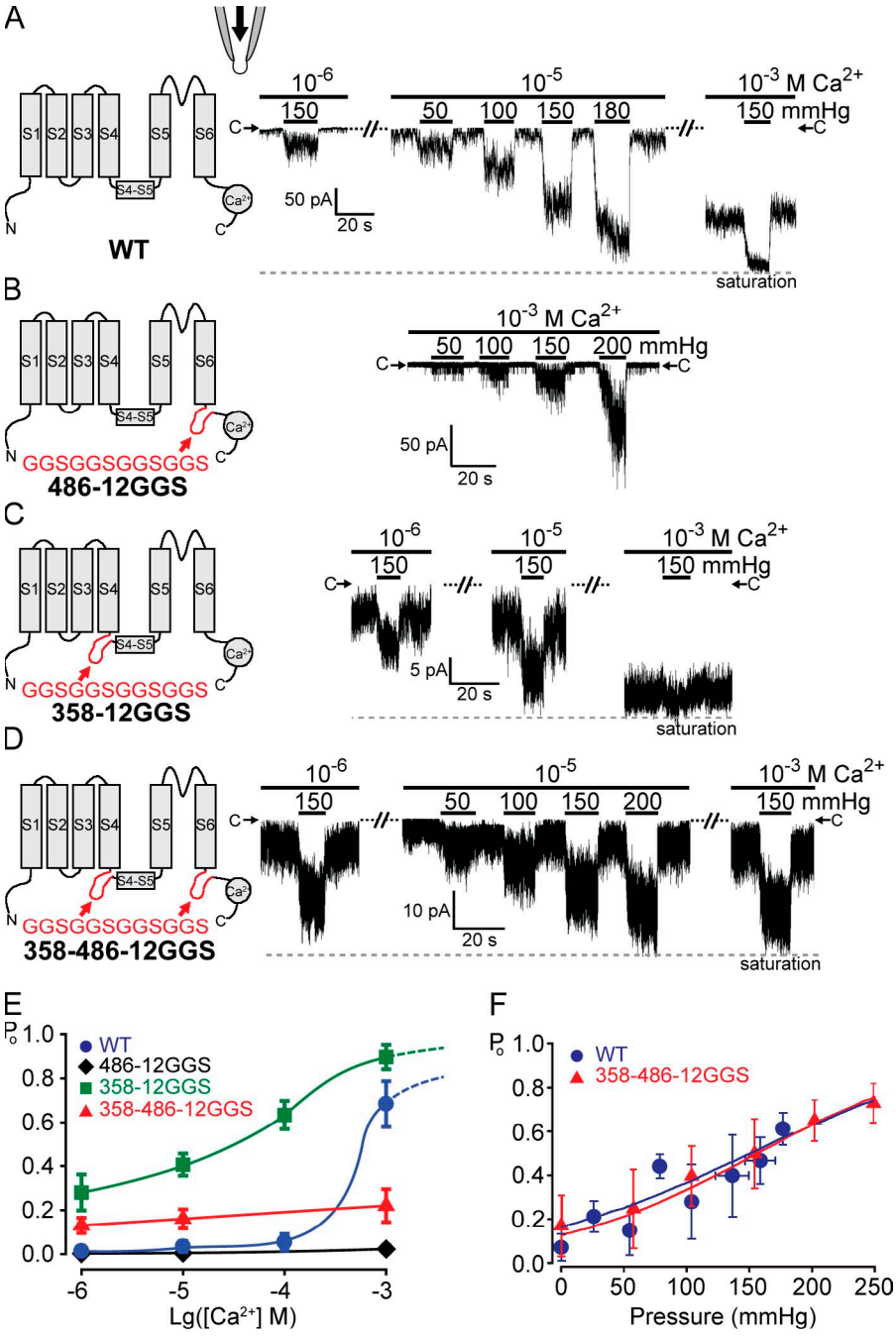

Figure 3. Inserting unstructured peptides before or after the S5–S6 core domain does not affect force activation. TRPY1 activities were examined in excised cytoplasmic-side-out patches bathed in the symmetric solution held at −50-mV driving inward currents. 10–20-s pressure pulses were delivered into the pipette to exert membrane stretch. (A, left) A diagram of one wild-type (WT) subunit showing S1 through S6, the S4–S5 linker, and a C-terminal Ca^{2+}-binding domain. (right) Typical traces of the wild-type–channel activities from one patch, bathed in low (10^{-6} M), intermediate (10^{-5}M), or high [Ca^{2+}] (10^{-3}M). At each [Ca^{2+}], different amounts of positive pressures were applied as depicted with black bars. Magnitudes of the pressure pulses in millimeters of Hg are labeled. C→ marks the closed current level; the dashed line marks the current maximum. Whereas basal activities increase with [Ca^{2+}], the increase in TRPY1 current upon pressure is clear in all [Ca^{2+}]s and is most evident at intermediate [Ca^{2+}] (10^{-5} M), where the basal activity is most suitable for the test of the force activation. (B–D) Diagrams and typical results of insertion mutants are arranged as in A. (B) 486-12GGS mutant with a 12-residue peptide (red) inserted at the C-terminal end of S6 greatly reduced Ca^{2+}-induced basal activities. Compare basal activities at high [Ca^{2+}] (10^{-3} M) between A and B. Nonetheless, pressure-induced responses are robust. (C) 358-12GGS with the 12-residue peptide inserted in front of the S4–S5 linker increased basal activities. Compare basal activities with those in A. Responses to pressure pulses are robust, though partially masked by high basal activities. (D) 358–486-12GGS with the peptide inserted at both sides of the S5–S6 core; pressure responses remain robust. Although A–D show results from typical cases, those from other patches (n = 20 for wild type and n = 6 each for 486-12GGS, 358-12GGS, and 358–486-12GGS) are highly consistent. (E) Plots of P_o versus [Ca^{2+}] showing a great reduction of the Ca^{2+} activation by the peptide insertion at position 486 (diamonds) and an elevation of the basal P_o by the insertion at position 358 (squares). 486-12GGS did not reach clear saturation even at high [Ca^{2+}] and under high pressure. Its P_o is thus normalized to the highest level we observed and will result in an overestimation. Means ± SD (n = 3 for all). (F) P_o versus pressure plots of wild type and 358–486-12GGS at 10^{-5} M Ca^{2+} fitted with the Boltzmann equation, the same as Fig. 1 B. Means ± SD (n = 6 for wild type and n = 4 for 358–486-12GGS). No clear difference in mechanosensitivity (Δα) can be discerned. See Table I. The low or high spontaneous activity of 486-12GGS or 358-12GGS, respectively, limited the accurate estimate of P_o or the test range of mechanosensitivity and cannot be plotted here.

sequences, lengths, and locations (Fig. 4). Channels with insertions between S6 and the C-terminal cytoplasmic domain all showed symptoms similar to that of 486-12GGS with greatly reduced Ca^{2+} activation but retention of robust force activation (Fig. 4, A and B). The effects of insertions after residue 358 (immediately before the S4–S5 linker) or after residue 363 (within the S4–S5 linker) were similar to that of 358-12GGS, being high in basal P_o (Fig. 4, C and D). Surprisingly, inserting GGSGGSGGSGGSGGSGGSGGSGGS at position 358 still produced functional channels, albeit at reduced expression levels. This 358-24GGS still displayed robust force activation (Fig. 4 D).

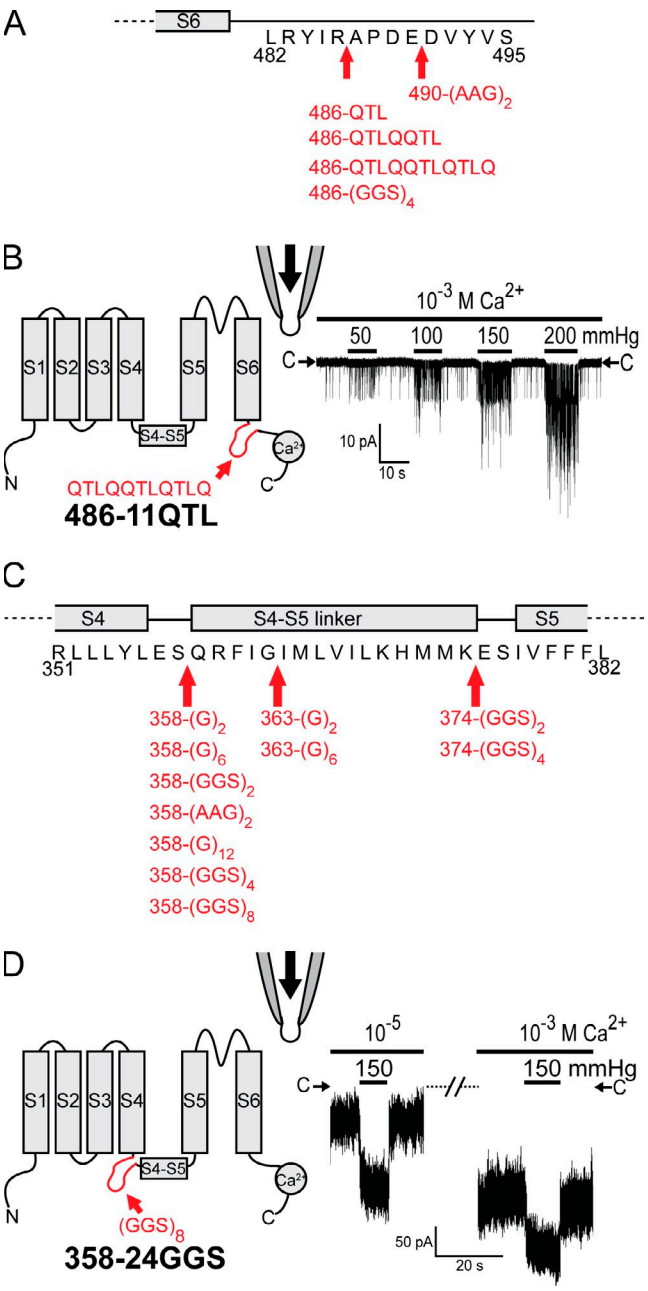

Figure 4. Various insertion mutants before or after the core domain do not affect force activation. (A and C) Diagrams showing insertions with different sequences, different lengths, and different locations. Insertion mutants with no observed functional channels are not depicted in the diagram, which include 369-6GGS, 372-6GGS, 373-6GGS, 375-6GGS, 376-6GGS, 377-6GGS, and 378-6GGS. (B and D) Similar diagrams and recording as in Fig. 3 of 486-11QTL and 358-24GGS, respectively.

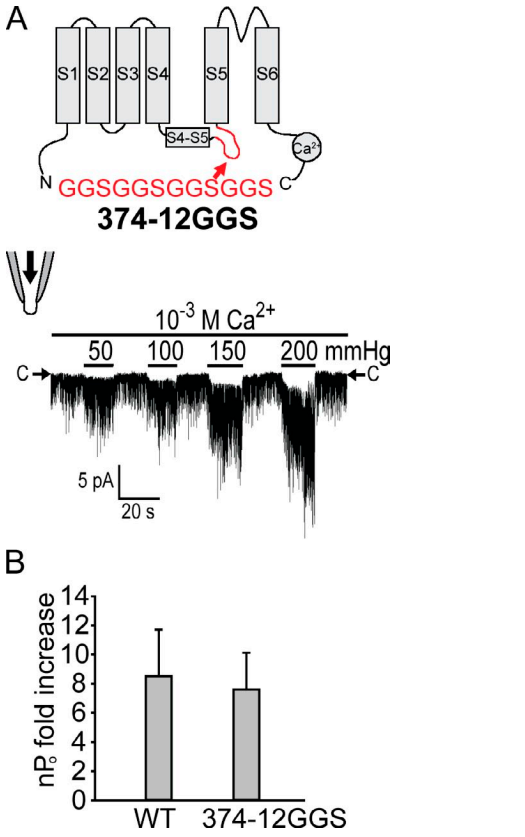

Figure 5. Inserting unstructured peptides between the S4–S5 linker and S5–S6 core domain does not much affect force activation. (A) A diagram and recording from 374-GGS are presented as in Fig. 3. This insertion shortens the open duration and thus lowers basal activities, which is evident when the activity at 10^{-3} M Ca^{2+} here and that of the wild type at the same $[Ca^{2+}]$ shown in Fig. 3 A are compared. (B) An over fivefold increase in nP_o observed in both the wild type and 374-12GGS upon 150-mmHg pressure. Because the saturation level could not be determined before lytic pressure even at high $[Ca^{2+}]$ because of its shortened open durations and less stable seal under high pressures compared with wild type, the quantification was conducted using the fold increase of nP_o stimulated by 150-mmHg pressure from comparable basal activity between 374-12GGS and wild type at different $[Ca^{2+}]$ (10^{-3} M for 374-12GGS and 10^{-5} M for wild type). No clear difference in mechanosensitivity can be discerned by this measure. P = 0.35. Means ± SD ($n = 3$ for both).

Peptide insertions between the S4–S5 linker and S5–S6 core

Similar to that of Kv, the amphipathic S4–S5 linker can associate with membrane, potentially sensing membrane force (Boukalova et al., 2010). An insertion at position 374, 374-12GGS, just after the S4–S5 linker where the S4–S5 linker contacts S6 in Kv, produced channels with decreased P_o at high $[Ca^{2+}]$ (10^{-3} M; Fig. 5 A) compared with that of wild type at the same $[Ca^{2+}]$ (Fig. 3, A and E). This mutant exhibited extremely short open durations, and its membrane could not withstand pressures as high as the wild type. Therefore, we could not determine the saturation level with confidence and consequently could not quantify its force activation with a $\Delta\alpha$ value. Instead, we measured the fold increase of nP_o stimulated by 150 mmHg of pressure from comparable basal activity between 374-12GGS and wild type at different $[Ca^{2+}]$ (10^{-3} M for 374-12GGS and 10^{-5} M for wild type; Fig. 5 B). By this measure, no significant difference in mechanosensitivity can be

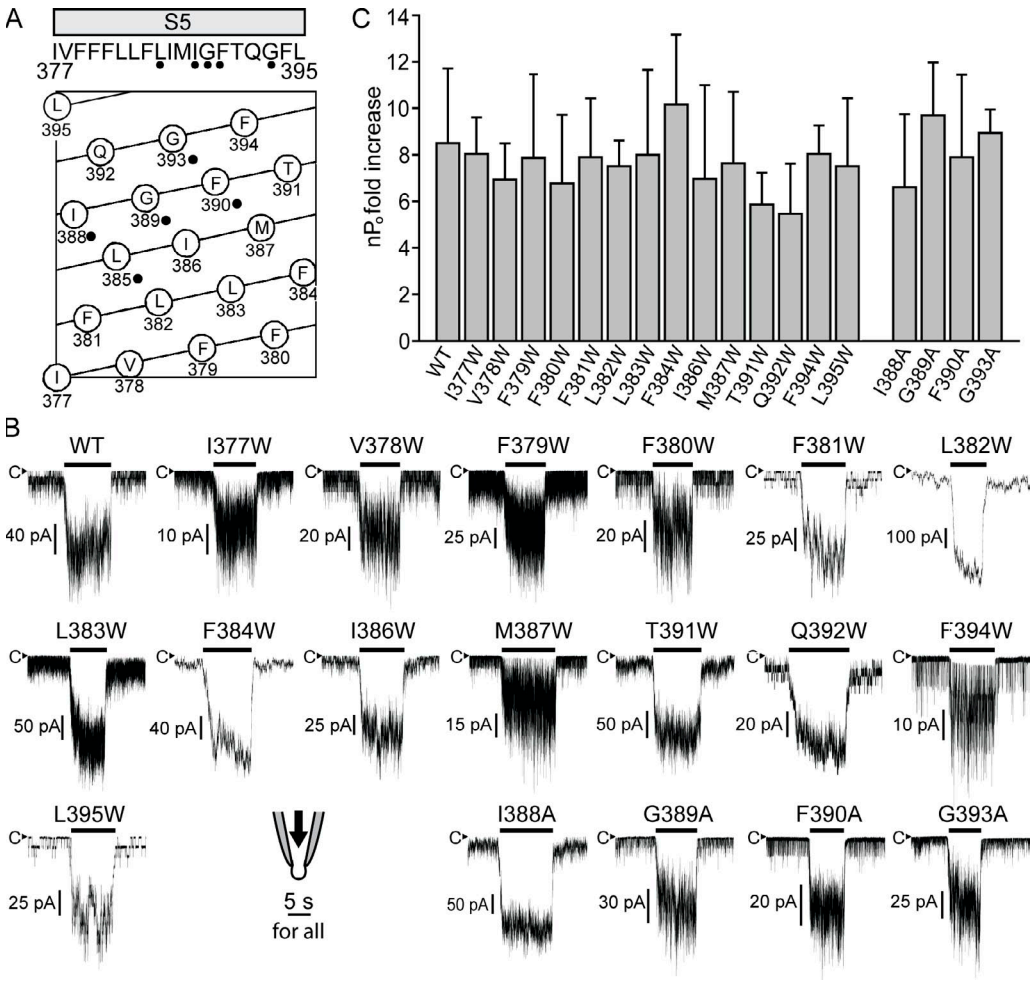

Figure 6. Tryptophan substitution mutants on S5 largely retain normal force activation. (A, top) A diagram of the S5 sequence. (bottom) A helical belt diagram produced by DNASTAR showing the relative amino acid positions on S5. Residues, the replacements of which with tryptophan produced constitutive channel activities, are labeled with black dots. Those were replaced with alanine for further analyses. (B) Representative traces of wild type (WT) and 14 tryptophan mutants and 4 alanine mutants showing robust force responses to 150-mmHg pressure. Whereas the wild type was tested at 10^{-5} M Ca^{2+}, the mutants were examined at different [Ca^{2+}] to better demonstrate their responses to pressure from appropriate basal activities, as many of these mutants affect basal activities and channel kinetics like the insertion mutants in Figs. 3 and 5. (C) Quantifications of the mechanosensitivity of wild type and mutants in B as the nP_o fold increase in response to 150-mmHg pressure. No significant difference can be discerned by this measure. $P > 0.05$. For those mutants whose saturation level could be determined, $\Delta\alpha$ values are compared with wild type in Fig. 7. Means ± SD ($n = 4$ for wild type and $n = 3$ for each mutant).

discerned between 374-12GGS and the wild type. This finding makes it unlikely that this S4–S5 linker (the Q359–K374 amphipathic helix) acts as a force sensor. As position 374 is at the kink between the linker and S5, it might be a critical residue if there is an interaction between the linker and S6 just like the case of Kv. Thus, inserting 12GGS here would disrupt such a noncovalent interaction as well as any signal transduction from S1–S4 through the linker.

Overall, all functional TRPY1 insertion mutants (Figs. 3–5) retained their responses to membrane stretch in excised patches. In cases where quantifications allow, the insertion mutants retain much of the mechanosensitivity (Fig. 3 F, Fig. 5 B, and Table I).

Perturbing possible noncovalent contacts between the S1–S4 and S5–S6 core by tryptophan and alanine substitutions does not significantly weaken TRPY1 force activation

In the crystal structures of Kv channels (Long et al., 2005a,b, 2007) and especially that of the bacterial ligand-regulated cation channel (Clayton et al., 2008), there are noncovalent contacts between S1–S4 and S5, attaching S1–S4 to the core domain. If TRPY1 is constructed similarly, these contacts may transmit force. We next investigated such possible noncovalent coupling from S1–S4 to the S5 shell of the core domain. Tryptophan has a bulky side chain. A replacement of an amino acid with tryptophan likely perturbs not only its own contact

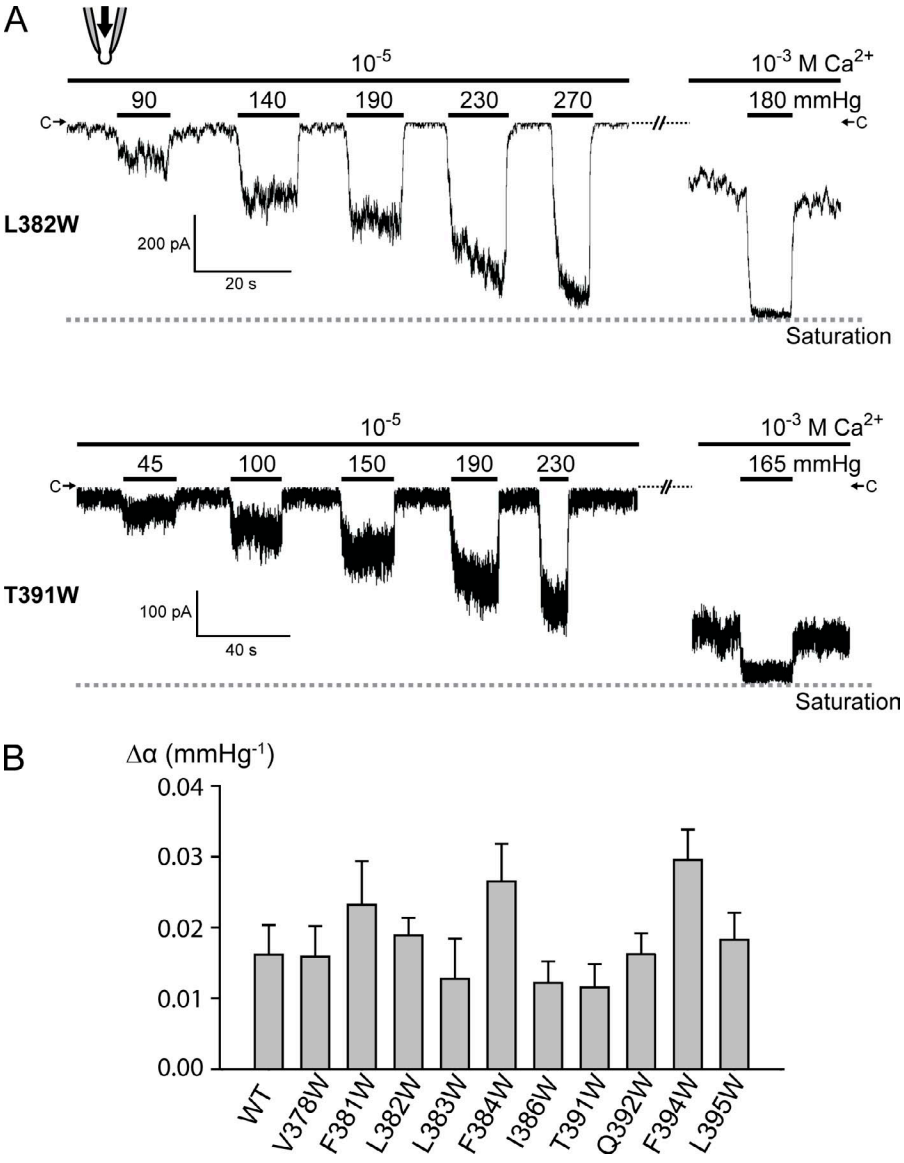

Figure 7. Tryptophan substitution mutants on S5 largely retain mechanosensitivity as quantified with Δα. (A) Similar recordings as in Fig. 3 of L382W and T391W showing representative tryptophan mutant channels whose saturation level can be determined at high [Ca^{2+}] under high pressure. (B) Δα extracted from a similar plot as in Fig. 1 B and Fig. 3 F were compared among wild type and 10 different tryptophan mutants on S5 whose saturation level can be determined at high [Ca^{2+}] under high pressure. See Materials and methods for the determination of the saturation level. None of the mutants show significantly reduced Δα, whereas F384W and F394W showed slightly increased Δα (between the wild type and 10 tryptophan mutants; $P > 0.05$ except for F384W and F394W). Means ± SD ($n = 6$ for wild type and $n = 3$ for each mutant).

points but also its local noncovalent contact networks if they exist. Tryptophan scanning mutagenesis, a commonly used method in channel research (Li-Smerin et al., 2000; Soler-Llavina et al., 2006), was therefore performed on the 19 S5 residues (377–395) of TRPY1 (Fig. 6 A). Among the 19 tryptophan mutants, L385W, I388W, G389W, F390W, and G393W (Fig. 6 A, black dots) are constitutively active, precluding a meaningful test of their force activation. The remaining 14 tryptophan mutants all retain overall similar responses to membrane stretch force as the wild type (Fig. 6, B and C; and Fig. 7). Except for I377W, F379W, F380W, and M387W, which exhibited characteristics similar to that of 374-12GGS (Fig. 5 A), precluding the determination of the channel saturation, the Δα values of the 10 remaining tryptophan mutants are similar to that of the wild type (Fig. 7 B). The five residues that yielded constitutively active tryptophan mutants were further analyzed with alanine substitutions. Except for L385A, which still remained overly active, the other four alanine mutants, I388A, G389A, F390A, and G393A, showed overall similar force activations as the wild type (Fig. 6, B and C).

DISCUSSION

Few MS TRP channels have been quantitatively scrutinized at the single-channel level. We have improved the techniques in recording of the yeast vacuolar membrane, making a quantitative examination of the behavior of TRPY1 possible. An added advantage is the ease of yeast molecular genetics that makes gene replacement at the native chromosomal locus a routine. Such replacements make the wild-type mutant comparisons direct, avoiding complexities encountered in the plasmid expression or random chromosomal insertion.

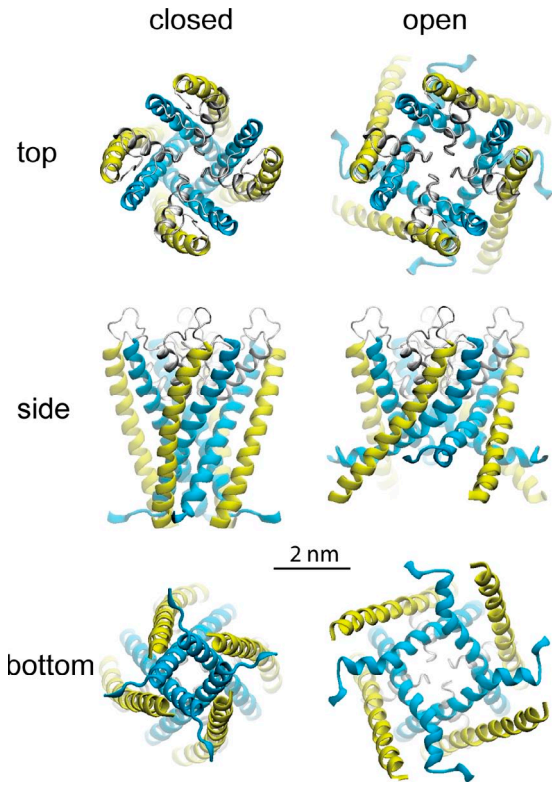

Figure 8. A homology model of the S5–S6 core domain of the TRPY1 channel to visualize the nature of the in-plane expansion upon opening. The computational model was constructed using the ROSETTA algorithm (Simons et al., 1997) based on limited homology between TRPY1 and K^+ channels (see supplemental information in Zhou et al., 2007). For clarity, only residues from 363 to 472 are shown as ribbons. Upon opening, both the external S5 helices (yellow) and the pore-lining S6 helices (blue) are modeled to bend, tilt, and expand driven by membrane tension.

Here, we take advantage of this experimental system toward understanding how mechanical force activates TRPY1. We have tried to uncouple its S5–S6 core from its surrounding structures. Around 30 strategic insertions or substitutions designed to disrupt communications of other modules with the core domain affect gating but do not remove TRPY1's mechanosensitivity, leading us to conclude that the TRPY1 core domain itself likely receives the mechanical force. We took this approach because several attempts to construct channels with the core alone or core-flank chimeras had failed (unpublished data). Concerns of this approach on whether or how well the insertions or substitutions uncouple the core are discussed below.

TRPY1 and its activities

TRP channels apparently evolved early in the eukaryotic lineage and form a large but loosely connected superfamily (Fig. S1 A). The animal TRP-A, -C, -M, -ML, -N, -P, and -V subfamilies have similarity only in their S5–S6 sequence. Microbial S5–S6 sequences are no less similar to the animal TRPs than among the animal TRPs themselves (Fig. S1 B). In fact, TRPY1, the yeast TRP, was cloned by recognizing this sequence (Palmer et al., 2001). It expresses a 320-pS unitary conductance in the vacuolar membrane, to which we have ready patch-clamp access (Palmer et al., 2001; Zhou et al., 2003). Animal TRPs are polymodal, integrating multiple physical and chemical stimuli and summing the various gating energies to activate (Latorre et al., 2007; Voets et al., 2007). TRPY1 also responds to several stimuli (Bertl and Slayman, 1990; Zhou et al., 2003), of which mechanical force and cytoplasmic Ca^{2+} are key (Fig. 1, A and B). These are not just parameters for biophysical evaluation but are biologically meaningful. Hyperosmotic shocks activate TRPY1 to release Ca^{2+} from the vacuole into the cytoplasm, as indicated by the fact that *trpy1* knockout shows no such release (Denis and Cyert, 2002). Osmotic activation of TRPY1 in vivo is readily explained by its activation by stretch force under patch clamp (Zhou et al., 2003). Ca^{2+} activation apparently forms a positive feedback as in other Ca^{2+}-dependent Ca^{2+} activations (Zhou et al., 2003). Previous (Su et al., 2009) and present experiments (Fig. 3, B and E; and Fig. 4, A and B) showed that Ca^{2+} activation of TRPY1 requires coupling between the S5–S6 core domain and the C-terminal cytoplasmic domain containing Ca^{2+}-binding sites (Fig. 1 A; Su et al., 2009).

TRPY1 is clearly activated by membrane stretch (Figs. 1–7; Zhou et al., 2003, 2007; Su et al., 2007, 2009). Our kinetic analysis shows that the force-sensitive step is from the interburst closed state to the burst (Fig. 2 and Table III). Compared with the bacterial channels MscL and MscS (Martinac, 2004), however, the mechanosensitivity of TRPY1 is weak, as seen in the shallow slope in the P_o-pressure plot in Fig. 1 B. This weaker mechanosensitivity corresponds to the small ΔA during the core expansion in the homology model (Fig. 8 and see section ΔA, the in-plane expansion of the core) and befits a polymodal channel that sums gating energies from several sources. Although TRPY1 is less impressive as a stretch-activated channel compared with those of bacteria, it is more representative of tetrameric cation channels, several of which have been shown to be stretch sensitive, including K_{2p}, Kv, Nav, etc. It is interesting to note that the interburst to burst transition step is also Ca^{2+} sensitive (unpublished data).

The efficacy of $(GGS)_n$ insertions

The rationale in our dissection here is that mutations tend to be destructive instead of constructive. They may therefore interfere with mechanosensitivity if placed in the path of force transmission. Whereas point substitution likely has small effects, large insertions may be more effective. Although we cannot be certain, long peptides like GGSGGSGGSGGS likely form unstructured loops that distort or disrupt α, β, or other secondary structures. Insertion of unstructured peptides immediately before

or after the TM5–TM6 core does not disrupt the peptide-backbone continuity but should slacken the covalent linkage. The fact that these insertions do not alter mechanosensitivity indicates that the mechanical stimulus is transmitted not through the stressed backbone but through either membrane tension acting directly on the S5–S6 core or through secondary interdomain interactions. The probability that force transmission remains in such structures through noncovalent contacts at the two insertion junctions seems remote. Such peptides have been used successfully to disrupt the communication between the S5–S6 core and the cytoplasmic Ca^{2+}-binding domain of the BK channel (Niu et al., 2004). Ca^{2+} activation of TRPY1 depends on a similar arrangement (Fig. 1 A; Su et al., 2009). The almost complete removal of Ca^{2+} sensitivity after the 486-12GGS insertion (Fig. 3, B and E) demonstrates that 12GGS insertion is indeed effective in disrupting the covalent linkage structures. Similar removal of Ca^{2+} sensitivity by the insertions of different peptides at residue 486 or 490 (Fig. 4 A) reinforces this conclusion. However, peptide insertions at different points flanking S5–S6 do not significantly affect activation by stretch force (Figs. 3–5), although they do affect gating (basal P_o and kinetics) because of their proximity to the gate. The 358-24GGS result is especially impressive. The 24-residue peptide inserted is as long as an entire transmembrane helix. It is formally possible that these unstructured peptide loops are able to disrupt the gating force of C-terminal Ca^{2+} binding but do not disrupt the mechanical gating force from the S1–S4 domains. However, it is difficult to envision how the mechanics can be so different for the C- and N-terminal covalent peptides immediately adjacent to the core. An alternative possibility is that transmission of mechanical force is through certain noncovalent contacts between the S1–S4 periphery and the S5–S6 core tested here with tryptophan substitutions. The simplest interpretation, however, is that the core itself senses the mechanical force. In crystal structures, the core domain of the Kv channel is directly exposed to membrane lipids (Long et al., 2007). TRPY1 may be arranged similarly, allowing it to sense the membrane force.

The efficacy of the tryptophan substitutions

Although multiple helical interactions between S1–S4 and S5 might possibly tolerate single tryptophan perturbations to some extent, single tryptophan mutants have been shown to be effective enough to strongly perturb the noncovalent interactions between S1–S4 and S5 in Kv (Li-Smerin et al., 2000; Soler-Llavina et al., 2006). Multiple tryptophan substitutions in a channel without a crystal structure in the hope of disrupting a function are impractical. Therefore, to the extent that can be experimentally addressed, our results that all testable single tryptophan or alanine mutants on S5 retain much of the force activation are consistent with the hypothesis that the noncovalent periphery–core contacts, if any, are not likely to be required for the major force transmission in TRPY1.

The mechanosensitivity of insertion or substitution mutants was quantified in two different measurements. For 358–486-12GGS (Fig. 3 F) and some tryptophan mutants (Fig. 7 B), their saturation levels and P_o can be determined as with the wild type (Fig. 3 A) by their response to high pressure at high $[Ca^{2+}]$ or by single-channel recordings. Thus, their $\Delta\alpha$ values are compared with that of wild type. For other mutants whose saturation level cannot be determined because of extremely low basal activities or drastic kinetics defects, we compared the nP_o-fold increases induced by 150 mmHg of pressure with that of wild type. These are the best quantifications allowed by this experimental system. Within the confidence imposed by variations of these experiments, we observed that all testable insertion and substitution mutants retain much of their mechanosensitivity and concluded that the core domain is the major force sensor of TRPY1.

ΔA, the in-plane expansion of the core

In the force activation, the product of the bilayer tension γ and the expansion coefficient ΔA (Fig. 1) is the energy that works to open the channel; this is analogous to the voltage and gating charges. We deduced ΔA from $\Delta\alpha$ of the Boltzmann curve (Fig. 1 B and Table I), where the transformation defines $P \times \Delta\alpha = \gamma \times \Delta A/k_B \times T$ based on Laplace's law (Fig. 1). We consistently observed the lytic pressure to be ~300 mmHg in the wild-type excised patches, and here we assume that it corresponds to the lytic tension (~10 mN/m) for excised patches (Suchyna et al., 2009). Therefore, a $\Delta\alpha$ of 0.015 approximately corresponds to a ΔA of 1.8 nm^2. In TREK1 that likely also senses membrane force directly, ΔA is found to be 4 nm^2 (Maksaev et al., 2011). For MscL, ΔA is reported as ~20 nm^2 (Chiang et al., 2004), much larger than that of eukaryotic channels. In MscL, force tilts and expands the transmembrane helices of its core domain (Sukharev et al., 2001; Kung, 2005; Kung et al., 2010), resulting in an in-plane area change from a closed to open state seen in the crystal structure ($\Delta A_{structure}$). $\Delta A_{structure}$ is predicted to be 23 nm^2 by structural models of MscL, which is consistent with its large ΔA value. We used the ROSETTA software (Simons et al., 1997) to model the pore domain of TRPY1 (see Materials and methods; Zhou et al., 2007). Although explicit membrane tension was not included in building the models (and future refinements in explicit bilayer might modify the structures to some extent), the templates used for the closed and open conformations predict an expansion area of $\Delta A_{structure}$ = ~2–4 nm^2 for the TRPY1 core, which is consistent with its experimental ΔA of 1.8 nm^2 that defines its mechanosensitivity. The general agreement of the

structural and functional estimate of ΔA allows us to propose that force activates TRPY1 by driving the in-plane area change of the core domain through pulling on S5–S6 transmembrane helices, like MscL. The smaller force-induced expansion in TRPY1 or TREK1 compared with that in MscL appears to reflect the physiological differences between eukaryotic and prokaryotic MS channels. Namely, MscL or MscS, which have large conductances, are used for massive solute evacuation to protect cells from osmotic lysis. MscL can pass not only all small ions but also all molecules <1,000 in molecular weight. In contrast, known eukaryotic MS channels are designed to have smaller conductances, to pass small ions only, and to benefit polymodal activation from other gating energies besides the mechanical force.

A common basis of mechanosensitivity?

Most biological membranes, when carefully examined, seem to have MS channels. Electrophysiologists often encounter force-activated channel currents of unknown origin. Many MS conductances, including stretch-activated channels, first described in 1984 (Guharay and Sachs, 1984), are of unclear molecular nature, although there are candidates (Coste et al., 2010). Although many eukaryotic MS channels underlying hearing, touch, etc. have yet to be identified, known MS channels are widespread among diverse channel families, including ENaC, K_{2P}, and TRP channels as well as those such as Kv, Nav, Cav, HCN2, BK, NMDA receptor, and even CFTR. Some seem to directly sense membrane tension, such as ENaC, TREK1, TRPY1, TRPV4, and NMDA receptor. These disparate MS channels share no recognizable force-sensing motifs with conserved protein sequences comparable with the well-recognized voltage-sensing domain or various ligand-binding pockets. However, being a channel entails having an ion pathway and a gate. For MscL, MscS, ENaC, K_{2P}, or NMDA receptor, the core domain is the only transmembrane module (Kung, 2005; Honoré, 2007; Kung et al., 2010). Thus, the core domain of those MS channels seems sufficient to sense membrane stretch force, at least in these cases. For TREK1 of the K_{2P} family, it has been reported that a C-terminal positively charged domain immediately following the core domain is crucial for its mechanosensitivity (Chemin et al., 2005). This domain may energetically contribute to the force sensing by the core through synergistic potentiation. If the channel core can sense membrane force, this would explain why so many different channel types are mechanosensitive. A further extension of this speculation is that the mechanosensitivity is a necessary physical consequence of being embedded in the highly anisotropic force environment of the lipid bilayer and may or may not be of physiological use. This makes force gating categorically different from well-studied voltage or ligand gating, where separate domains sense those stimuli. However, it remains possible that some channels are designed such that their cores, unlike Kv, are not exposed to lipids. In such cases, force may be transmitted to the gate through other domains or subunits, including cytoskeletons. We need to investigate many more channel types thoroughly for a full understanding.

The authors thank Stephen H. Loukin and Xinliang Zhou for critical comments and advice throughout the work.

This work was supported by National Institutes of Health grants GM 54867 to Y. Saimi and RO3 GM125020 to C. Kung.

Kenton J. Swartz served as editor.

Submitted: 22 July 2011
Accepted: 7 November 2011

REFERENCES

Arnadóttir, J., and M. Chalfie. 2010. Eukaryotic mechanosensitive channels. *Annu Rev Biophys.* 39:111–137. http://dx.doi.org/10.1146/annurev.biophys.37.032807.125836

Bertl, A., and C.L. Slayman. 1990. Cation-selective channels in the vacuolar membrane of *Saccharomyces*: dependence on calcium, redox state, and voltage. *Proc. Natl. Acad. Sci. USA.* 87:7824–7828. http://dx.doi.org/10.1073/pnas.87.20.7824

Beyder, A., J.L. Rae, C. Bernard, P.R. Strege, F. Sachs, and G. Farrugia. 2010. Mechanosensitivity of Nav1.5, a voltage-sensitive sodium channel. *J. Physiol.* 588:4969–4985. http://dx.doi.org/10.1113/jphysiol.2010.199034

Booth, I.R., M.D. Edwards, S. Black, U. Schumann, and S. Miller. 2007. Mechanosensitive channels in bacteria: signs of closure? *Nat. Rev. Microbiol.* 5:431–440. http://dx.doi.org/10.1038/nrmicro1659

Boukalova, S., L. Marsakova, J. Teisinger, and V. Vlachova. 2010. Conserved residues within the putative S4-S5 region serve distinct functions among thermosensitive vanilloid transient receptor potential (TRPV) channels. *J. Biol. Chem.* 285:41455–41462. http://dx.doi.org/10.1074/jbc.M110.145466

Calabrese, B., I.V. Tabarean, P. Juranka, and C.E. Morris. 2002. Mechanosensitivity of N-type calcium channel currents. *Biophys. J.* 83:2560–2574. http://dx.doi.org/10.1016/S0006-3495(02)75267-3

Chalfie, M. 2009. Neurosensory mechanotransduction. *Nat. Rev. Mol. Cell Biol.* 10:44–52. http://dx.doi.org/10.1038/nrm2595

Chemin, J., A.J. Patel, F. Duprat, I. Lauritzen, M. Lazdunski, and E. Honoré. 2005. A phospholipid sensor controls mechanogating of the K+ channel TREK-1. *EMBO J.* 24:44–53. http://dx.doi.org/10.1038/sj.emboj.7600494

Chiang, C.S., A. Anishkin, and S. Sukharev. 2004. Gating of the large mechanosensitive channel in situ: estimation of the spatial scale of the transition from channel population responses. *Biophys. J.* 86:2846–2861. http://dx.doi.org/10.1016/S0006-3495(04)74337-4

Christensen, A.P., and D.P. Corey. 2007. TRP channels in mechanosensation: direct or indirect activation? *Nat. Rev. Neurosci.* 8:510–521. http://dx.doi.org/10.1038/nrn2149

Clayton, G.M., S. Altieri, L. Heginbotham, V.M. Unger, and J.H. Morais-Cabral. 2008. Structure of the transmembrane regions of a bacterial cyclic nucleotide-regulated channel. *Proc. Natl. Acad. Sci. USA.* 105:1511–1515. http://dx.doi.org/10.1073/pnas.0711533105

Coste, B., J. Mathur, M. Schmidt, T.J. Earley, S. Ranade, M.J. Petrus, A.E. Dubin, and A. Patapoutian. 2010. Piezo1 and Piezo2 are essential components of distinct mechanically activated cation channels. *Science.* 330:55–60. http://dx.doi.org/10.1126/science.1193270

Cui, J., and R.W. Aldrich. 2000. Allosteric linkage between voltage and Ca(2+)-dependent activation of BK-type mslo1 K(+)

channels. *Biochemistry.* 39:15612–15619. http://dx.doi.org/10.1021/bi001509+

Denis, V., and M.S. Cyert. 2002. Internal Ca^{2+} release in yeast is triggered by hypertonic shock and mediated by a TRP channel homologue. *J. Cell Biol.* 156:29–34. http://dx.doi.org/10.1083/jcb.200111004

Gu, C.X., P.F. Juranka, and C.E. Morris. 2001. Stretch-activation and stretch-inactivation of Shaker-IR, a voltage-gated K+ channel. *Biophys. J.* 80:2678–2693. http://dx.doi.org/10.1016/S0006-3495(01)76237-6

Guharay, F., and F. Sachs. 1984. Stretch-activated single ion channel currents in tissue-cultured embryonic chick skeletal muscle. *J. Physiol.* 352:685–701.

Ho, S.N., H.D. Hunt, R.M. Horton, J.K. Pullen, and L.R. Pease. 1989. Site-directed mutagenesis by overlap extension using the polymerase chain reaction. *Gene.* 77:51–59. http://dx.doi.org/10.1016/0378-1119(89)90358-2

Honoré, E. 2007. The neuronal background K2P channels: focus on TREK1. *Nat. Rev. Neurosci.* 8:251–261. http://dx.doi.org/10.1038/nrn2117

Kloda, A., L. Lua, R. Hall, D.J. Adams, and B. Martinac. 2007. Liposome reconstitution and modulation of recombinant N-methyl-D-aspartate receptor channels by membrane stretch. *Proc. Natl. Acad. Sci. USA.* 104:1540–1545. http://dx.doi.org/10.1073/pnas.0609649104

Kung, C. 2005. A possible unifying principle for mechanosensation. *Nature.* 436:647–654. http://dx.doi.org/10.1038/nature03896

Kung, C., B. Martinac, and S. Sukharev. 2010. Mechanosensitive channels in microbes. *Annu. Rev. Microbiol.* 64:313–329. http://dx.doi.org/10.1146/annurev.micro.112408.134106

Latorre, R., S. Brauchi, G. Orta, C. Zaelzer, and G. Vargas. 2007. ThermoTRP channels as modular proteins with allosteric gating. *Cell Calcium.* 42:427–438. http://dx.doi.org/10.1016/j.ceca.2007.04.004

Lin, W., U. Laitko, P.F. Juranka, and C.E. Morris. 2007. Dual stretch responses of mHCN2 pacemaker channels: accelerated activation, accelerated deactivation. *Biophys. J.* 92:1559–1572. http://dx.doi.org/10.1529/biophysj.106.092478

Li-Smerin, Y., D.H. Hackos, and K.J. Swartz. 2000. A localized interaction surface for voltage-sensing domains on the pore domain of a K+ channel. *Neuron.* 25:411–423. http://dx.doi.org/10.1016/S0896-6273(00)80904-6

Long, S.B., E.B. Campbell, and R. Mackinnon. 2005a. Crystal structure of a mammalian voltage-dependent Shaker family K+ channel. *Science.* 309:897–903. http://dx.doi.org/10.1126/science.1116269

Long, S.B., E.B. Campbell, and R. Mackinnon. 2005b. Voltage sensor of Kv1.2: structural basis of electromechanical coupling. *Science.* 309:903–908. http://dx.doi.org/10.1126/science.1116270

Long, S.B., X. Tao, E.B. Campbell, and R. MacKinnon. 2007. Atomic structure of a voltage-dependent K+ channel in a lipid membrane-like environment. *Nature.* 450:376–382. http://dx.doi.org/10.1038/nature06265

Loukin, S., X. Zhou, Z. Su, Y. Saimi, and C. Kung. 2010. Wild-type and brachyolmia-causing mutant TRPV4 channels respond directly to stretch force. *J. Biol. Chem.* 285:27176–27181. http://dx.doi.org/10.1074/jbc.M110.143370

Lundbæk, J.A., P. Birn, A.J. Hansen, R. Søgaard, C. Nielsen, J. Girshman, M.J. Bruno, S.E. Tape, J. Egebjerg, D.V. Greathouse, et al. 2004. Regulation of sodium channel function by bilayer elasticity: the importance of hydrophobic coupling. Effects of Micelle-forming amphiphiles and cholesterol. *J. Gen. Physiol.* 123:599–621. http://dx.doi.org/10.1085/jgp.200308996

Lundbæk, J.A., R.E. Koeppe II, and O.S. Andersen. 2010. Amphiphile regulation of ion channel function by changes in the bilayer spring constant. *Proc. Natl. Acad. Sci. USA.* 107:15427–15430. http://dx.doi.org/10.1073/pnas.1007455107

Maksaev, G., A. Milac, A. Anishkin, H.R. Guy, and S. Sukharev. 2011. Analyses of gating thermodynamics and effects of deletions in the mechanosensitive channel TREK-1: comparisons with structural models. *Channels (Austin).* 5:34–42.

Martinac, B. 2004. Mechanosensitive ion channels: molecules of mechanotransduction. *J. Cell Sci.* 117:2449–2460. http://dx.doi.org/10.1242/jcs.01232

Morris, C.E., and P.F. Juranka. 2007. Nav channel mechanosensitivity: activation and inactivation accelerate reversibly with stretch. *Biophys. J.* 93:822–833. http://dx.doi.org/10.1529/biophysj.106.101246

Niu, X., X. Qian, and K.L. Magleby. 2004. Linker-gating ring complex as passive spring and Ca(2+)-dependent machine for a voltage- and Ca(2+)-activated potassium channel. *Neuron.* 42:745–756. http://dx.doi.org/10.1016/j.neuron.2004.05.001

Palmer, C.P., X.L. Zhou, J. Lin, S.H. Loukin, C. Kung, and Y. Saimi. 2001. A TRP homolog in *Saccharomyces cerevisiae* forms an intracellular Ca(2+)-permeable channel in the yeast vacuolar membrane. *Proc. Natl. Acad. Sci. USA.* 98:7801–7805. http://dx.doi.org/10.1073/pnas.141036198

Sachs, F. 2010. Stretch-activated ion channels: what are they? *Physiology (Bethesda).* 25:50–56. http://dx.doi.org/10.1152/physiol.00042.2009

Sakmann, B., and E. Neher, editors. 1983. Single-channel Recording. Plenum Press, New York. 503 pp.

Schmidt, D., and R. MacKinnon. 2008. Voltage-dependent K+ channel gating and voltage sensor toxin sensitivity depend on the mechanical state of the lipid membrane. *Proc. Natl. Acad. Sci. USA.* 105:19276–19281. http://dx.doi.org/10.1073/pnas.0810187105

Sharif-Naeini, R., J.H. Folgering, D. Bichet, F. Duprat, I. Lauritzen, M. Arhatte, M. Jodar, A. Dedman, F.C. Chatelain, U. Schulte, et al. 2009. Polycystin-1 and -2 dosage regulates pressure sensing. *Cell.* 139:587–596. http://dx.doi.org/10.1016/j.cell.2009.08.045

Shcherbatko, A., F. Ono, G. Mandel, and P. Brehm. 1999. Voltage-dependent sodium channel function is regulated through membrane mechanics. *Biophys. J.* 77:1945–1959. http://dx.doi.org/10.1016/S0006-3495(99)77036-0

Simons, K.T., C. Kooperberg, E. Huang, and D. Baker. 1997. Assembly of protein tertiary structures from fragments with similar local sequences using simulated annealing and Bayesian scoring functions. *J. Mol. Biol.* 268:209–225. http://dx.doi.org/10.1006/jmbi.1997.0959

Soler-Llavina, G.J., T.H. Chang, and K.J. Swartz. 2006. Functional interactions at the interface between voltage-sensing and pore domains in the Shaker K(v) channel. *Neuron.* 52:623–634. http://dx.doi.org/10.1016/j.neuron.2006.10.005

Su, Z., X. Zhou, W.J. Haynes, S.H. Loukin, A. Anishkin, Y. Saimi, and C. Kung. 2007. Yeast gain-of-function mutations reveal structure-function relationships conserved among different subfamilies of transient receptor potential channels. *Proc. Natl. Acad. Sci. USA.* 104:19607–19612. http://dx.doi.org/10.1073/pnas.0708584104

Su, Z., X. Zhou, S.H. Loukin, Y. Saimi, and C. Kung. 2009. Mechanical force and cytoplasmic Ca(2+) activate yeast TRPY1 in parallel. *J. Membr. Biol.* 227:141–150. http://dx.doi.org/10.1007/s00232-009-9153-9

Suchyna, T.M., V.S. Markin, and F. Sachs. 2009. Biophysics and structure of the patch and the gigaseal. *Biophys. J.* 97:738–747. http://dx.doi.org/10.1016/j.bpj.2009.05.018

Sukharev, S.I., P. Blount, B. Martinac, and C. Kung. 1997. Mechanosensitive channels of *Escherichia coli*: the MscL gene, protein, and activities. *Annu. Rev. Physiol.* 59:633–657. http://dx.doi.org/10.1146/annurev.physiol.59.1.633

Sukharev, S., M. Betanzos, C.S. Chiang, and H.R. Guy. 2001. The gating mechanism of the large mechanosensitive channel MscL. *Nature.* 409:720–724. http://dx.doi.org/10.1038/35055559

Voets, T., K. Talavera, G. Owsianik, and B. Nilius. 2005. Sensing with TRP channels. *Nat. Chem. Biol.* 1:85–92. http://dx.doi.org/10.1038/nchembio0705-85

Voets, T., G. Owsianik, A. Janssens, K. Talavera, and B. Nilius. 2007. TRPM8 voltage sensor mutants reveal a mechanism for integrating thermal and chemical stimuli. *Nat. Chem. Biol.* 3:174–182. http://dx.doi.org/10.1038/nchembio862

Vriens, J., H. Watanabe, A. Janssens, G. Droogmans, T. Voets, and B. Nilius. 2004. Cell swelling, heat, and chemical agonists use distinct pathways for the activation of the cation channel TRPV4. *Proc. Natl. Acad. Sci. USA.* 101:396–401. http://dx.doi.org/10.1073/pnas.0303329101

Zhang, W.K., D. Wang, Y. Duan, M.M. Loy, H.C. Chan, and P. Huang. 2010. Mechanosensitive gating of CFTR. *Nat. Cell Biol.* 12:507–512. http://dx.doi.org/10.1038/ncb2053

Zhao, H.C., H. Agula, W. Zhang, F. Wang, M. Sokabe, and L.M. Li. 2010. Membrane stretch and cytoplasmic Ca2+ independently modulate stretch-activated BK channel activity. *J. Biomech.* 43:3015–3019. http://dx.doi.org/10.1016/j.jbiomech.2010.06.018

Zhou, X.L., A.F. Batiza, S.H. Loukin, C.P. Palmer, C. Kung, and Y. Saimi. 2003. The transient receptor potential channel on the yeast vacuole is mechanosensitive. *Proc. Natl. Acad. Sci. USA.* 100:7105–7110. http://dx.doi.org/10.1073/pnas.1230540100

Zhou, X., Z. Su, A. Anishkin, W.J. Haynes, E.M. Friske, S.H. Loukin, C. Kung, and Y. Saimi. 2007. Yeast screens show aromatic residues at the end of the sixth helix anchor transient receptor potential channel gate. *Proc. Natl. Acad. Sci. USA.* 104:15555–15559. http://dx.doi.org/10.1073/pnas.0704039104